Date of publication xxxx 00, 0000, date of current version xxxx 00, 0000.

Digital Object Identifier 10.1109/ACCESS.2017.DOI

Low-Profile Beam Steerable Patch Array with SIW Feeding Network

YU-JIE LIU, QIAO CHENG, AHSAN NOOR KHAN, HENRY GIDDENS, MAX MUNOZ TORRICO AND YANG HAO, (FELLOW, IEEE)

School of Electronic Engineering and Computer Science, Queen Mary University of London, E1 4NS, UK

Corresponding author: Yang Hao (e-mail: y.hao@qmul.ac.uk).

This work was supported by the IET AF Harvey Research Prize awarded to Professor Yang Hao.

ABSTRACT This paper presents a novel beam steerable array antenna that encompasses fully planar, low profile and lightweight characteristics for satellite communication (SatCom) applications. The proposed array contains a wideband linear source generator (LSG), an array of circular patches, and an inductive surface. The LSG is designed based on the substrate-integrated-waveguide (SIW) technology, whereas the patches are regarded as coupling circular scatterers, placed on the inductive surface for converting surface wave into the radiating wave. Each scatterer acts as a location-dependent phaser that can tailor the farfield behaviour to leverage beam steering, and is achieved by changing its distribution mechanically. A prototype of the proposed design has been fabricated and measured to evaluate the antenna performance. The measured results are in good agreement with the simulated results. The array antenna operates well with $S_{11} <$ -10 dB in the frequency band of 10.75-12.5 GHz and has stable radiation performance with beam steering capability of nearly $\pm 60^{\circ}$ in the elevation plane. The total height of the proposed array is about 5.1 mm ($0.19\lambda_{\circ}$). It is envisaged that the proposed antenna array will empower small moving platforms due to low cost, low profile and suitability for mass production.

INDEX TERMS Array antenna, beam steering, low-profile, satellite communication, substrate-integrated waveguide (SIW).

I. INTRODUCTION

CURRENTLY, there is an increasing demand for establishing seamless, uninterrupted and high data rate wireless connections for satellite communication [1]. A relative low-profile antenna system is thus required to enable wireless communications with a wide-angle scanning capability [2]. During the last few decades, various established solutions have been explored to realize such antennas with low apertures and broad scanning capabilities. In [3], an integrated circuit (ICs) based stacked patch array antenna was proposed to obtain the steering capability of $\pm 60^{\circ}$. The array profile was significantly reduced by implementing the principle of folded reflectarray [4], [5] that incorporated a reflector based polarization grid. Another planar array [6] was designed within one functional block using an RF circuitry and dual-band scanning performances were achieved using digital beam steering concept [7], [8]. Some other planar antennas also integrated with active devices to obtain electronic steering [9], [10]. For this reason, these electronically scanning arrays have been considered as the future of mobile communication terminals [11]. However, feeding networks with the ICs or digital phase shifters are expensive and raise major concerns for commercial users as they can be cumbersome, lossy and complicated to design for large array antennas [12].

In recent years, research has been devoted to assimilating electrical and mechanical scanning capabilities together [13] and replacing the costly phase shifters with electrically controllable materials, such as Liquid Crystal [14]. In [15], Kymeta developed a Metamaterial Surface Antenna Technology (MSAT) based on a holographic concept and integrated with liquid crystals as on-or-off switches, which enabled the antenna to achieve $\pm 60^{\circ}$ beam scanning at a total thickness of 50 mm. Nevertheless, this technique requires a sophisticated algorithm for optimizing the desired metasurface in addition to extra microchip components such as field-programmable gate arrays (FPGA), and thus it becomes expensive for SatCom operators [12]. Furthermore, despite the reduced cost, the MSAT also involves complicated assembly and is therefore, like other hybrid phased arrays, not suitable for

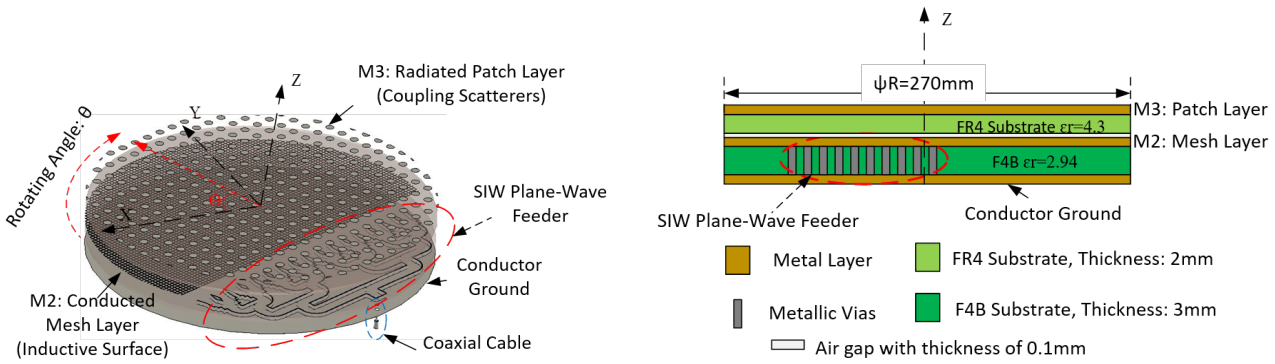

FIGURE 1: The details of the proposed array antenna with: (a) Perspective view, (b) Cross-sectional view.

mass production [16], [17].

The continuous transverse stub (CTS) antenna is a low cost, low profile antenna solution for SatCom applications. It has significant advantages in the low-cost feeding mechanisms and mechanical steering system, obviating the need for any expensive active phase devices. CTS antennas were invented in the 1990s by Milroy [18]. Usually, a CTS array consists of a set of 1-D long radiating slots and a broadband line source that support the fundamental transverse electromagnetic (TEM) mode. Its far-field characteristics can be tailored by rotating the in-between relative positions of the radiating slots and line source. Later on, Milroy continued to derive the variable inclination CTS (VICTS) array [19] for scanning capabilities. In [20], a gap waveguide fed VICTS array was proposed in the 60 GHz band that has achieved steering range up to $\pm 60^{\circ}$ within the thickness of 9.35 mm (1.92 λ_0). A CTS array with a high aperture efficiency of 60% was presented in [21] with a rotating feed part. This technique excludes the requirements of a radiating aperture and ensues in leveraging array with $\pm 30^{\circ}$ and frequency independent beam directions. Although several types of CTS arrays have been implemented to target specific applications [22], their metallic waveguide structures are massive and still require high power mechanical control systems to realize scanning in azimuth and elevation planes. The mechanical control system also makes the whole antenna system bulky and consumes more power that is not feasible for low-cost applications. Furthermore, an external polarizer is required to maintain the consistent polarization of VICTS array due to its dependence on the directions of radiating slots under rotation.

In this paper, we propose a novel low profile array that integrates several critical emerging antenna technologies for SatCom applications. The proposed design addresses the constraints of complex feeding networks and costly phase shifters; the design process does not require algorithmic programming techniques as that have been utilized for electronic and hybrid beam steering array antennas. The use of substrate integrated waveguide (SIW) feeding and radiating patch elements on PCB materials provide mass production possibility with low-cost processing, and also significantly reduces the antenna weight. In contrary to existing VICTS antenna solutions, the proposed approach offers more freedom of integrating active components or designing the radiating elements without influencing the plane-wave feeder, as the inductive surface isolates it from the radiating layer. In the VICTS antenna, it is not easy to achieve these co-design characteristics without altering the feeding performance. Furthermore, this design utilizes circular coupling scatterers to achieve consistent linear polarisation without requiring any extra external polarizers.

The remainder of this paper is organized as follows. In Section II, the antenna architecture and its working principle will be described. Section III presents the broadband SIW line source generator (LSG) for the antenna prototype, and simulated results are briefly illustrated. A detailed characterization of the antenna through simulated and measured results is explained in Section IV, along with a comparison of SatCom array antennas from the literature.

II. ANTENNA DESIGN AND ANALYSIS

A. OPERATION PRINCIPLE AND 1-D ARRAY ANTENNA DESIGN

The proposed array is developed from the phased array sheet concept [25] and implemented into Ku band specifically for SatCom applications. It is well known that the 2D guided surface wave is converted into a 3D radiating beam in free space with the wavenumber modulation. The directivity is dependent on the grating period of each scatterer (or antenna element) [26]. Fig. 1 illustrates the array structure in detail. From the perspective view, a 50 Ω coaxial cable is used to connect the SIW, and the SIW plane-wave feeder, which is constructed by combining power divider with the multiple T-junctions, generates the line source for the array. A conductive mesh layer, known as inductive surface (labelled as M2), is designed for the surface wave propagating at the interface of two substrates with different permittivity [27]. The circular scatterers (labelled as M3) are utilized to couple the surface wave energy into free-space radiation with

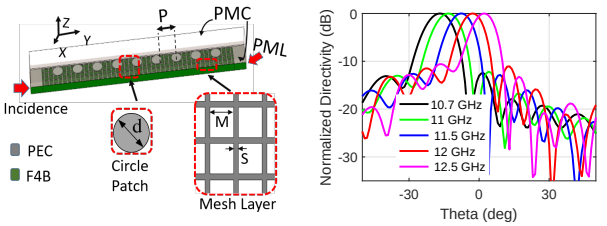

(a) (b)

FIGURE 2: (a) Simulation model of 1D array with 9 circular patch elements as the scatterers. The details of the dimensions are M = 2.5 mm, S = 0.5 mm, d = 6.6 mm, P = 13.3 mm. (b) Simulated results of normalized radiation patterns of the 1D-array at various frequencies.

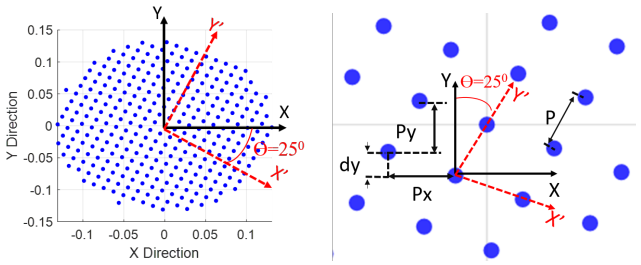

(a) (b)

FIGURE 3: The equivalent array distribution with the dynamic coordination system shown in red dash line. (a) When the M3 layer is relatively rotated by θ = 25°. (b) The variation of element spacing in X and Y directions under the condition of rotating angle θ = 25°, where $P_x = P_y = P\cos(\theta)$ and $d_y = P\sin(\theta)$.

consistent polarization. Fig. 1(b) shows the cross-sectional view which consists of 5 layers - 3 conductive layers and 2 substrates. M3 layer is etched on the top surface of an FR-4 substrate with a thickness of 2 mm. Beneath the FR-4, another metal M2 layer is located with both the inductive surface and a SIW plane-wave feeder in F4B dielectric with a permittivity of 2.94 and thickness of 3 mm. The beam scanning feature is achieved by rotating M3 layer in relative to the bottom layer. Each of the scatterers has a varying phase delay which is dependent on the rotation angle. This position is expressed through the rotating angle (RA) referred as the angle between the X-axis, as shown in Fig. 1(a). In order to avoid the interfacial friction while rotating, an air gap with 0.1 mm space is needed between M2 layer and FR-4 substrates. The whole antenna has a diameter of 270 mm and a thickness of 5.1 mm, equivalent to just 0.19 $\lambda_\circ$.

A periodic model of a 1-D array was built to investigate the surface-to-plane wave conversion and is illustrated in Fig. 2(a). The sidewalls were set as perfect magnetic conductor (PMC) boundary conditions in order to maintain the plane wave propagation. When the incident plane-wave propagates along the y-direction in the SIW, the non-radiative evanescent field is formed on the inductive surface. This field simultaneously propagates in the y-direction and decays exponentially along z-direction. The scatterers on the top layer perturb this evanescent field condition, and some portion of the guided evanescent energy is coupled into magnetic dipole like radiation. A mesh of conductive lines can realize the inductive surface with the period (e.g. M = 2.5 mm) and line width (e.g. S = 0.5 mm), which both are sufficiently shorter than the guided wavelength (e.g: λ_g = 16.35 mm) at 10.7 GHz. Its theory was described in [28] with details. The scatterers diameter (e.g. d = 6.6 mm) is calculated and optimized according to the microstrip antenna method [29]. The spacing between each scatterer is about one wavelength (e.g. $p = \lambda_s$ = 13.36 mm) in the FR-4 dielectric for achieving the in-phase radiation. Meanwhile, the simulated radiation patterns, in Fig. 2(b), verify the above working scenario at the frequencies of 10.7 GHz, 11 GHz, 11.5 GHz, 12 GHz and 12.5 GHz, which indicate that the designed array antenna works well in the SatCom receiving bandwidth of 10.7 to 12.5 GHz.

B. THEORETICAL MODEL FOR ARRAY PATTERN

Rather than utilizing the frequency scanning capability, the antenna design mainly focusses on the beam steering capabilities across different frequencies. As stated above, rotating the upper M3 layer provides the required phased delay to realize beam scanning, as the relative element period changes along with it. Here, the equivalent radiation model is analyzed with a theoretical calculation to obtain the array beam patterns. Fig. 3 illustrates the equivalent circular element distribution of this proposed array while the rotating angle (RA) is at θ = 25°. By referring to the closed-form solution of the VICTS array [25], [30], the main beam of this proposed array is therefore predictable.

As shown in Fig. 3(b), the locations of the elements can be expressed as:

$$X_{mn} = mP_x, \tag{1}$$

$$Y_{mn} = nP_y + md_y. \tag{2}$$

where m and n are integers. By assuming each element has the same coupled amplitude, and each of them is approximately radiating as an isotropic point source in the farfield, the antenna pattern can be calculated as follows

$$AF(\theta,\varphi) \backsimeq \frac{e^{j\beta_0 R}}{R}\sum_{m,n}\sqrt{r(1-r)^n} \times e^{-jm(\beta_0 P_y \sin(\theta)\cos(\varphi)-\beta_g P_y)} \times e^{-jn[\beta_0(d_y \sin(\theta)\cos(\varphi)+P_x \sin(\theta)\sin(\varphi))-\beta_g d_y]}. \tag{3}$$

Here, r is a coupled energy rate. λ_g and λ_0 are the wavelength in the SIW and in the air, respectively. R is the distance from the center element to the far observation point which can be indicated as:

$$\theta = \sin^{-1}(\sqrt{u^2+v^2}), \tag{4}$$

$$\varphi = tan^{-1}(\frac{v}{u}). \tag{5}$$

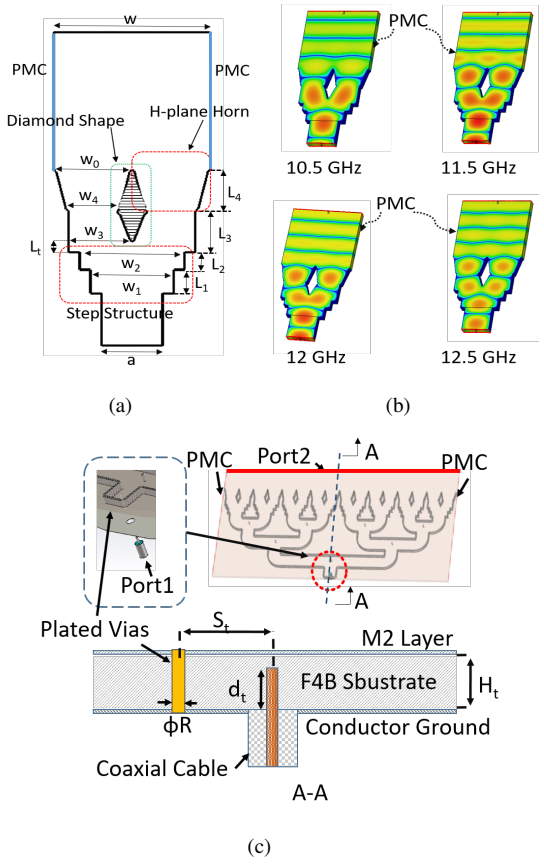

FIGURE 4: (a) SIW T-junction configuration which transfer the TE mode into quasi-TEM mode with dimension details, (b)E-field distribution at the frequencies of 10.5 GHz, 11.5 GHz, 12 GHz and 12.5 GHz, (c)The structure of the LSG which contains the 1-to-8 power divider and 8 T-junctions and also with the feeding details of coaxial cable to SIW design. The used parameters are listed in Table 1.

where u and v are defined below:

$$u = \frac{(P_y - \lambda_g)\lambda_0}{P_x P_y}, \tag{6}$$

$$v = \frac{d_y \lambda_0}{P_x P_y}. \tag{7}$$

As $P_x = P_y = P\cos(\theta)$ and $d_y = P\sin(\theta)$ are all relative to the rotating angle θ and fix element spacing P, the location of the main beam is easily calculated through the Eq. 4 and 5. The theoretical antenna radiation results are compared with the simulated and measured results later in the paper (Table 2).

III. DESIGN OF SIW LINE SOURCE GENERATOR

The LSG is one of the critical parts for the array antenna, and its key point is to launch a plane wave in the parallel-plate waveguide. There are already various types of SIW-LSG have been developed in recent decades. For example, the series structure with a cascade of π junctions [31], and parabolic cylindrical reflector based on geometrical optics [23], [24]. Taking into account the design considerations of achieving the required bandwidth and utilizing simple low-cost fabrication techniques, we utilized a SIW-LSG design by arranging a series of H-plane horns together to achieve plane wave propagation. As shown in Fig. 4(a), the proposed T-junction design contains two H-plane horns and one 1-to-2 power divider. The sidewalls of it are set as PMC boundary to imitate the infinite space for the plane-wave propagation. It is worth noting that the plane-wave propagation is highly dependent on the coupling between adjacent H-plane horns, which requires the width (e.g. w_0) of the H-plane horn to be about one dielectric wavelength (e.g. λ_g) at the highest frequency of 12.5 GHz in the SIW. We explicitly design the 1-to-2 power divider to connect the above H-plane horns. For proper impedance matching, the diamond-shaped divider and the step structure are applied to efficiently transfer the waveguide mode to parallel-plate mode with a compact size, where the lengths (e.g. L_3, L_4) are approximately $0.5\lambda_g$ at a centre frequency of 11.5 GHz. The E-field distributions at frequencies of 10.5 GHz, 11.5 GHz, 12 GHz and 12.5 GHz displayed in Fig. 4(b) indicate that this designed T-junction can convert the TE mode to quasi-TEM mode perfectly across the operating bandwidth.

Fig. 4(c) shows the whole structure of the proposed LSG, including the detail of connecting to coaxial cable. Eight T-junctions are linked with the power divider and placed serially together to obtain the full range plane-wave in SIW. Through the equations in [32], the SIW parameters, of ϕR, the plated vias radius, and V_d, the periodic spacing, can be easily calculated for gaining excellent transmission effi-

TABLE 1: Dimensions of The Line Source Generator (Unit: mm)

$\mathbf{w}$	$\mathbf{w}_0$	$\mathbf{w}_1$	$\mathbf{w}_2$	$\mathbf{w}_3$	$\mathbf{w}_4$
27.8	13.9	14.82	18.64	11.25	9.08
$\mathbf{L}_1$	$\mathbf{L}_2$	$\mathbf{L}_3$	$\mathbf{L}_4$	$\mathbf{L}_t$	$\mathbf{a}$
4.55	3.32	7.72	7.57	2.1	10.82
$\mathbf{d}_t$	$\mathbf{S}_t$	$\mathbf{H}_t$	$\phi\mathbf{R}$	V_d	
2.5	3.77	3	0.94	1.2	

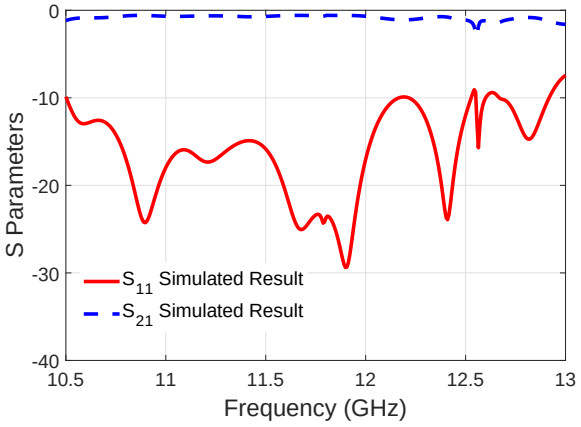

FIGURE 5: LSG simulated results including amplitudes of reflection (S_{11}) and transmission (S_{21}) coefficients.

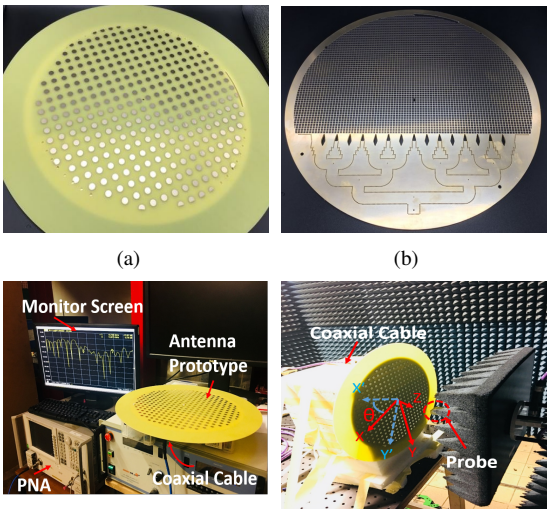

FIGURE 6: The photographs of (a) the top scatterers layer, (b) the bottom feeding network, (c) the antenna prototype and its S-parameter measurement setup and (d) the near-field setup for pattern measurement.

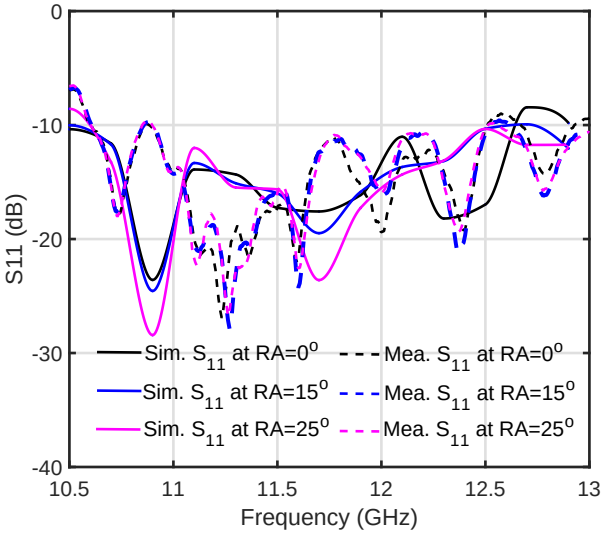

FIGURE 7: The reflection coefficient comparison at the rotating angle (RA) of 0°, 15° and 25° between simulated and measured results.

ciency. The coaxial cable connection part was also optimized in order to have a sufficient transmission. The inner core of the connector was embedded into the substrate at a length of 2.5 mm, and the feeding position is placed away from the SIW bottom border at a distance of $S_t = \lambda_g/4$ in the SIW. The final parameters of the LSG structure are listed in Table 1. Fig. 5 illustrates the simulated S-parameter of LSG with both amplitudes of reflection and transmission coefficients, which shows that the LSG transmission with S_{11} below -10 dB, whilst there is less than 0.5 dB transmission loss during the bandwidth of 10.5 GHz to 12.5 GHz.

IV. ARRAY ANTENNA PROTOTYPE AND ITS CHARACTERIZATION RESULTS

In order to validate this proposed array design, a prototype with a total of 313 patch scatterers was manufactured using a low-cost PCB processing technology. The bottom substrate is a double-sided copper-clad, laminated with gold plating. The high conductivity can reduce the loss of surface wave propagation on the inductive surface. The top layer of circular scatterers is shown in Fig. 6(a) and the SIW feeding network with inductive mesh are shown in 6(b). In addition, Fig. 6(c) and 6(d) also show the S-parameter and radiation pattern measurement setup with N5244A PNA-X Network Analyzer and NSI 2D near-field scanner system, respectively. The simulated and measured reflection coefficients at different rotating angles are shown in Fig. 7. The reflection coefficient remains below -10 dB across the entire 10.75-12.5 GHz band (a relative bandwidth of 15%) and is unaffected by the rotational angles.

Fig. 8 shows the measured normalized radiation patterns at rotating angles (RAs) of 0°, 10°, 15°,20° and 25° and frequencies of 11.5 GHz, 12 GHz and 12.5 GHz. The simulated radiation patterns at three RAs are also displayed for comparison. A relatively good agreement can be observed between them. In the measurement, the beam steering range has achieved from 0° to 53° at 12.5 GHz. The side-lobe level (SLL) remains -10 dB below the maximum at most of the rotating angles except the angle at 25°. This increased SLL is due to a larger reflected surface wave at the high rotating angle. Further details on the scanning angle and SLL for rotation angles of 15° and 25° are listed in Table 2, including the data at 11 GHz which shows a steering angle of 60° was achieved.

The antenna gain and radiation efficiency at various rotating angles are shown in Fig. 9. It can be observed that the measured gains remain stable with reduced beam scanning loss in the RA range from 0° to 20°, in which the maximum scanned angle reaches 45° at 11.5 GHz within 1 dB gain difference. Comparing to the simulated gain at RA that equals to 0°, the measured gain is with the average lower value of 2.8 dB. This gain reduction is attributed to substrate material loss and fabrication tolerance because the F4-B dielectric has a high loss tangent above 10 GHz, and it was used to manufacture the feeding structure. Also, the upper FR-4 substrate would have an impact on the antenna gain as it is a well-known lossy material. The FR-4 was used here to generate the surface wave at the interface of two materials, and these two substrates should have a different permittivity [27]. In this case, FR-4 is a suitable option as the permittivity is different as compared to F4-B, and it has some advantages in price compared to low loss RF PCB substrates. Likewise, this material loss causes radiation efficiency to decrease from 65% in simulation to 40% in measurement. And the measured radiation efficiency continues decreasing as the frequency increases above 10 GHz, which illustrated in Fig. 9. Despite these losses, a 70% efficiency is achieved

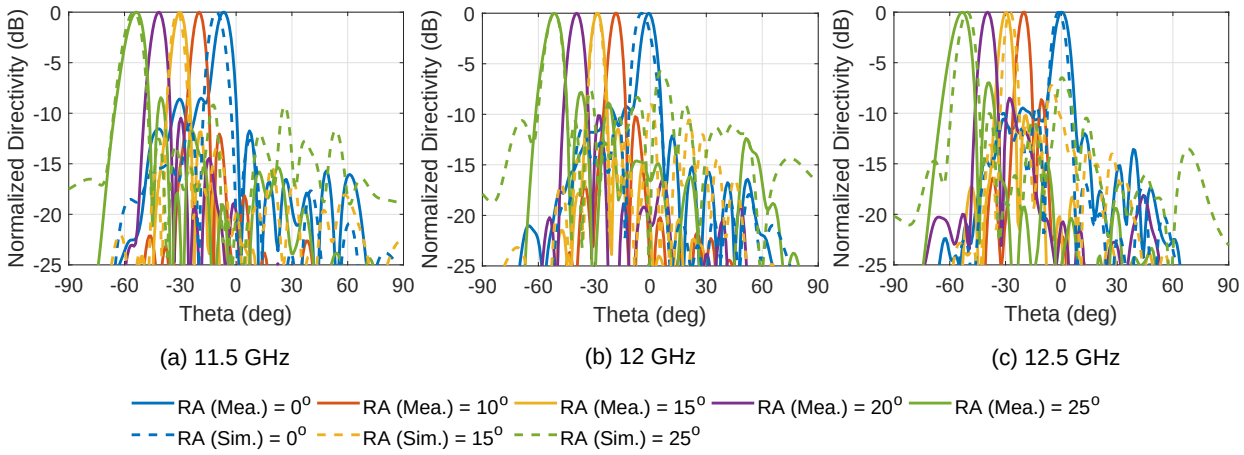

FIGURE 8: **Measured and simulated radiation patterns of this beam steerable proposed Array at 11.5 GHz, 12 GHz and 12.5 GHz. Solid lines show the measured directivity at Rotating Angle (RA) of 0°,10°,15°,20° and 25°, and dash lines represent the simulated results at RA of 0°, 15° and 25°.**

TABLE 2: **The Details of Radiation Patterns of the proposed Array Antenna. ('The.' stands for Theoretical)**

	Rotating Angle at 15°					Rotating Angle at 25°				
	Scanned Angle (°)			SLL(dB)		Scanned Angle (°)			SLL(dB)	
Freq (GHz)	Mea.	Sim.	The.	Mea.	Sim.	Mea.	Sim.	The.	Mea.	Sim.
11	-36	-34	-38	-11	-15	-60	-58	-68	-8	-9.2
11.5	-34	-32	-34	-12	-16	-58	-55	-60	-9	-12.5
12	-33	-29	-31	-11.5	-14	-56	-53	-54	-8	-11
12.5	-30	-28	-28	-10	-12	-53	-51	-50	-7	-10

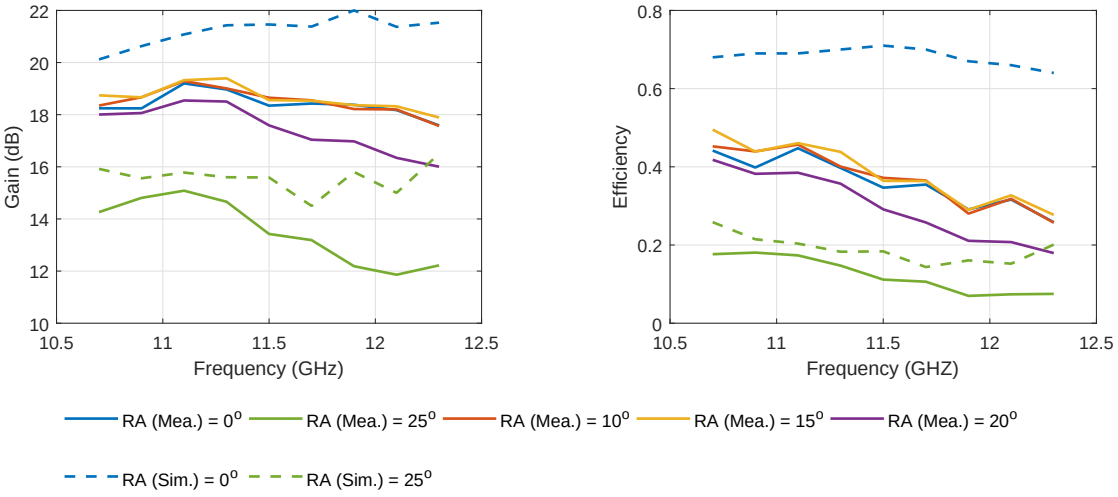

FIGURE 9: **Simulated and measrued realized gain and efficiency comparisons at different rotating angles (RAs).**

for RA = 0° in simulation, which indicates that the antenna efficiency could be improved with low loss substrate, and this should be considered for a commercial exploitation.

Besides, in Fig. 9, a relatively significant gain drop of 5 dB has been observed at the rotating angle of 25°. This gain drop is attributed to the increased spacing between scatterers with the rotating movement, resulting in a decreased number of radiating elements, and less surface mode energy is transferred into a radiation mode. This also leads to the high SLL occurred along with the increased reflective wave. It can be clarified that at this phrase, the proposed array scans to 45° within the gain reduction of 2 dB, and the gain drops to 5 dB

TABLE 3: The Performance Comparisons of different types of steerable Array Antennas

Ref.	Type	Bandwidth	Scanning Range (°)	Height	Aperture Dimension	Peak Gain (dBi)
[3]	Folded-Reflector	4.3%	60	$0.29\lambda_0$	$5.52\lambda_0 \times 5.52\lambda_0$	5.8
[7]	Patch Array	16.4%	70	$0.11\lambda_0$	$7.58\lambda_0 \times 8.47\lambda_0$	N/A
[13]	Hybrid	4%	60	$9.19\lambda_0$	$9.33\lambda_0 \times 2.33\lambda_0$	36
[14]	Liquid Crystal	8.3%	30	$0.07\lambda_0$	$2.37\lambda_0 \times 1.42\lambda_0$	6
[19] [20]	VICTS (WG)	13%	60	$1.9\lambda_0$	$17\lambda_0 \times 17\lambda_0$	29.3
This Work	Grating Array (SIW)	15%	60	$0.19\lambda_0$	$8.62\lambda_0 \times 6\lambda_0$ (exclude network)	19.5

while the scanned angle is above 60°. It is a concern that this gain drop and high SLL have caused the radiation efficiency reduces below 20%, and higher power may be needed to reach the SatCom signal in some areas. It is worth noting that VICTS array also suffers from the same reflective wave issue. To overcome this issue, the authors in [19] applied the RF choke to reduce its robust reflective wave. This RF choke presents an extremely high impedance to any incidences and generated magnitude interference between reflective and transmitted waves. However, this RF choke requires a very good mechanical processing which significantly increases the cost and complexity of the manufacturing. Nevertheless, the fully planar and isolated feeder characteristics of our approach do, however offer the possibility to alleviate the aforementioned issues. With emerging metasurface features, it is possible to eliminate the coupling effect while increasing the numbers of radiating elements and enhance the antenna gain and efficiency at a sizeable rotating angle. For example, by integrating a resistive surface as a perfectly matched layer or absorber at the end of the plane-wave feeder, one can alleviate the reflective wave issue straightforward with low-cost fabrication in contrast to the VICTS array. This will be conducted in future work.

Finally, Table 3 summarizes the performances of the current published beam steering array solutions for SatCom applications. Electrical ICs or digital beam steering enabled technologies that have been used in planar array design offer a very low profile and wide scanning range [3], [7]. However, they still suffer from the complex feeding networks, which lead to low antenna gain and high cost in scaling to larger arrays. Another patch array which integrates liquid crystal beam steering avoids the lossy network but has limited steering range [14] or requires extra FPGA for algorithm programming [15]. Meanwhile, the hybrid [13] and VICTS arrays [20] have the highest radiation efficiency, but they both suffer from bulky mechanical control systems which have been built with metalized waveguides. In terms of weight and assembly, the proposed array antenna has the advantages of low weight, easier assembly and package. The proposed array is low profile and has achieved comparable scanning performance. The fabrication of the proposed antenna is particularly suitable for mass production and can be further scaled to a larger aperture with cost-efficient LSG feeding network. Overall, this proposed array antenna solution has the potential with integrating active/passive components for specific applications, like Radar Cross-section (RCS) reductions, and low-cost attractive contributions to satellite communication on small moving platforms.

V. CONCLUSION AND DISCUSSION

In this paper, a novel beam steerable array antenna with low-cost SIW feeding network has been presented for the Ku-band SatCom applications. The proposed antenna has been successfully validated using the SIW technologies and PCB process. The theoretical, simulated and measured results of radiation patterns have excellent agreement among each other. The bandwidth of reflection coefficient for S_{11}<-10 dB is around 15% in measurements for all rotating angles. The $\pm 60°$ scanning capability and peak gain of 19.5 dBi have been obtained at this designed bandwidth. Although the array side-lobe levels (SLLs) need some improvements, it is still worthy of conducting further work to fulfil and develop for practical use. This developed array antenna solution is an up-and-coming candidate for the satellite communication on the small moving platforms where low cost, low profile, easy assembly and integration are required.

REFERENCES

[1] E. Feltrin and E. Weller, "New frontiers for the mobile satellite interactive services," 2010 5th Advanced Satellite Multimedia Systems Conference and the 11th Signal Processing for Space Communications Workshop, Cagliari, 2010, pp. 155-161.

[2] Y. Rahmat-Samii and A. C. Densmore, "Technology Trends and Challenges of Antennas for Satellite Communication Systems," in IEEE Transactions on Antennas and Propagation, vol. 63, no. 4, pp. 1191-1204, April 2015.

[3] T. Chaloun, V. Ziegler and W. Menzel, "Design of a Dual-Polarized Stacked Patch Antenna for Wide-Angle Scanning Reflectarrays," in IEEE Transactions on Antennas and Propagation, vol. 64, no. 8, pp. 3380-3390, Aug. 2016.

[4] Y. Ge, C. Lin and Y. Liu, "Broadband Folded Transmitarray Antenna Based on an Ultrathin Transmission Polarizer," in IEEE Transactions on Antennas and Propagation, vol. 66, no. 11, pp. 5974-5981, Nov. 2018.

[5] Q. Luo et al., "Antenna array elements for Ka-band satellite communication on the move," 2013 Loughborough Antennas and Propagation Conference (LAPC), Loughborough, 2013, pp. 135-139.

[6] E. Meniconi, V. Ziegler, R. Sorrentino and T. Chaloun, "3D integration technologies for a planar dual band active array in Ka-band," 2013 European Microwave Conference, Nuremberg, 2013, pp. 215-218.
[7] A. H. Aljuhani, T. Kanar, S. Zihir and G. M. Rebeiz, "A Scalable Dual-Polarized 256-Element Ku-Band Phased-Array SATCOM Receiver with $\pm$ 70° Beam Scanning," 2018 IEEE/MTT-S International Microwave Symposium - IMS, Philadelphia, PA, 2018, pp. 1203-1206.
[8] D. Sikri and R. M. Jayasuriya, "Multi-Beam Phased Array with Full Digital Beamforming for SATCOM and 5G," Microwave Journal, Vol. 62, Issue 4, PP. 64-79, April, 2019.
[9] S. Vaccaro, D. L. del Rio, J. Padilla and R. Baggen, "Low cost Ku-band electronic steerable array antenna for mobile satellite communications," Proceedings of the 5th European Conference on Antennas and Propagation (EUCAP), Rome, 2011, pp. 2362-2366.
[10] M. Tripodi, F. DiMarca, T. Cadili, C. Mollura, F. DiMaggio and M. Russo, "Ka band active phased array antenna system for satellite communication on the move terminal," Proceedings of the 5th European Conference on Antennas and Propagation (EUCAP), Rome, 2011, pp. 2628-2630.
[11] L. Marcellini, R. Lo Forti and G. Bellaveglia, "Future developments trend for Ku and Ka antenna for satcom on the move," Proceedings of the 5th European Conference on Antennas and Propagation (EUCAP), Rome, 2011, pp. 2346-2350.
[12] C. Henry, "Satellite operators view antennas as weak link in broadband business plans," July 7, 2018. [Online]. Available: https://spacenews.com/satellite-operators-view-antennas-as-weak-link-in-broadband-business-plans/.
[13] G. Han, B. Du, W. Wu and B. Yang, "A Novel Hybrid Phased Array Antenna for Satellite Communication on-the-Move in Ku-band," in IEEE Transactions on Antennas and Propagation, vol. 63, no. 4, pp. 1375-1383, April 2015.
[14] J. Shu, G. Xu, H. Peng and J. Mao, "An Electrically Steerable Parasitic Array Radiator in Package Based on Liquid Crystal," in IEEE Antennas and Wireless Propagation Letters, vol. 18, no. 11, pp. 2365-2369, Nov. 2019.
[15] R. Stevenson, M. Sazegar, A. Bily, M. Johnson and N. Kundtz, "Metamaterial surface antenna technology: Commercialization through diffractive metamaterials and liquid crystal display manufacturing," 2016 10th International Congress on Advanced Electromagnetic Materials in Microwaves and Optics (METAMATERIALS), Chania, 2016, pp. 349-351.
[16] F. Tiezzi, S. Vaccaro, D. Llorens, C. Dominguez and M. Fajardo, "Ku-band hybrid phased array antennas for mobile satellite communication systems," 2013 7th European Conference on Antennas and Propagation (EuCAP), Gothenburg, 2013, pp. 1605-1608.
[17] S. Borisov and A. Shishlov, "Antennas for Satcom-on-the-Move, Review," 2014 International Conference on Engineering and Telecommunication, Moscow, 2014, pp. 3-7.
[18] W. W. Milroy, "Continuous Transverse Stub (CTS) Element Devices and Methods of Making Same," U.S. Patent 5266961, Aug.29, 1991.
[19] W. W. Milroy, J. Sor and E. Yum, "Augmented E-Plane Taper Techniques in Variable Inclination Continuous Transverse (VICTS) Antennas," U.S. Patent 9413073 B2, Aug.9, 2016.
[20] K. Tekkouk, J. Hirokawa, R. Sauleau and M. Ando, "Wideband and Large Coverage Continuous Beam Steering Antenna in the 60-GHz Band," in IEEE Transactions on Antennas and Propagation, vol. 65, no. 9, pp. 4418-4426, Sept. 2017.
[21] X. Lu, S. Gu, X. Wang, H. Liu and W. Lu, "Beam-Scanning Continuous Transverse Stub Antenna Fed by a Ridged Waveguide Slot Array," in IEEE Antennas and Wireless Propagation Letters, vol. 16, pp. 1675-1678, 2017.
[22] T. Lou, X. Yang, H. Qiu, Z. Yin and S. Gao, "Compact Dual-Polarized Continuous Transverse Stub Array With 2-D Beam Scanning," in IEEE Transactions on Antennas and Propagation, vol. 67, no. 5, pp. 3000-3010, May 2019.
[23] X. Yang, L. Di, Y. Yu and S. Gao, "Low-Profile Frequency-Scanned Antenna Based on Substrate Integrated Waveguide," in IEEE Transactions on Antennas and Propagation, vol. 65, no. 4, pp. 2051-2056, April 2017.
[24] Y. Gao, T. Hong, W. Jiang, S. Gong and F. Li, "Low-Profile Wideband CTS Array Using Substrate-Integrated Waveguide Technology for K-Band Applications," in IEEE Transactions on Antennas and Propagation, vol. 67, no. 8, pp. 5711-5716, Aug. 2019.
[25] Y. Monnai and H. Shinoda, "Microwave phased array sheet for wireless sensor network," 2010 Seventh International Conference on Networked Sensing Systems (INSS), Kassel, 2010, pp. 123-129.
[26] Y. Monnai and H. Shinoda, "Converting 2D microwave into 3D beam using dielectric grating antenna," 2009 Sixth International Conference on Networked Sensing Systems (INSS), Pittsburgh, PA, 2009, pp. 1-5.
[27] F. K. Schwering and Song-Tsuen Peng, "Design of Dielectric Grating Antennas for Millimeter-Wave Applications," in IEEE Transactions on Microwave Theory and Techniques, vol. 31, no. 2, pp. 199-209, Feb. 1983
[28] H. Shinoda, Y. Makino, N. Yamahira and H. Itai, "Surface Sensor Network Using Inductive Signal Transmission Layer," 2007 Fourth International Conference on Networked Sensing Systems, Braunschweig, 2007, pp. 201-206.
[29] K. Carver and J. Mink, "Microstrip antenna technology," in IEEE Transactions on Antennas and Propagation, vol. 29, no. 1, pp. 2-24, January 1981.
[30] B. G. Porter, "Closed form expression for antenna patterns of the Variable Inclination Continuous Transverse Stub," 2010 IEEE International Symposium on Phased Array Systems and Technology, Waltham, MA, 2010, pp. 164-169.
[31] J. Hirokawa and M. Ando, "Single-layer feed waveguide consisting of posts for plane TEM wave excitation in parallel plates," in IEEE Transactions on Antennas and Propagation, vol. 46, no. 5, pp. 625-630, May 1998.
[32] Z. Kordiboroujeni and J. Bornemann, "Designing the Width of Substrate Integrated Waveguide Structures," in IEEE Microwave and Wireless Components Letters, vol. 23, no. 10, pp. 518-520, Oct. 2013.